scientific reports

Check for updates

OPEN

Open-closed conduit transitions regulate the large magnitude explosive eruptions of Petrazza, PaleoStromboli I (Stromboli, Italy)

E. Nicotra[1]✉, M. Minniti[1,2], F. Ridolfi[3], R. Sulpizio[4,5,6], C. A. Tranne[7] & F. Lucchi[7]✉

A multi-disciplinary approach of volcano-stratigraphy, petrology and geochemistry has shed light on the pre-eruptive processes, the eruptive triggering, behaviour and the architecture of the magma plumbing system during the explosive cycle of Petrazza at ca. 77–75 ka (PaleoStromboli I eruptive epoch, Stromboli). This was the largest magnitude eruptive cycle in Stromboli and one of the largest of the entire Aeolian archipelago, able to produce Vulcanian to sub-Plinian/Plinian phases with distal deposits found in the tephrostratigraphic record of the Tyrrhenian sea and surroundings. Our study highlighted that, differently from the present-day activity, the large magnitude Petrazza eruptive cycle could be attributed to phases of closed-system conditions, as also testified by the in equilibrium presence of amphibole, indicative of a "steady-state" magmatic status of the system. The explosive activity is then attributed to strong depressurization underwent by the plumbing system due to the cyclic closure/opening of the shallow conduit, possibly also in association with lateral collapse events. As shown by textural and compositional studies on plagioclase crystals, this decompression was also able to recall amphibole bearing mafic magma from the deep portion of the plumbing system (5–15 km of depth).

Keywords Magma plumbing system, Eruption triggering, Volcano stratigraphy, Pre-eruptive processes, Stromboli

The definition of triggering mechanisms of volcanic eruptions represents one of the major challenges in modern volcanology, as this is strictly connected with the consequent actions to be taken in terms of Civil Protection plans of mitigation and reduction of volcanic risk. As timescales of direct observation of eruptive phenomena are very different from those of geological processes, one of the best ways to gain insights on eruptive mechanisms and processes is volcano stratigraphy, along with sedimentological, geochemical, petrographical and petrological investigations. This approach may provide an outlook on most of the processes acting on the volcanic system, from those occurring in the magma plumbing system prior and during the eruption to the processes of fragmentation up to the mechanisms of transport and deposition.

The island of Stromboli is a largely submerged, (mainly) mafic composite volcano located in the north-eastern sector of the Aeolian volcanic arc (Southern Tyrrhenian Sea, Italy; Fig. 1). It is famous for its almost perennial strombolian activity, at least during the last 1200 years, characterized by low- to medium-energy explosive activity erupting shoshonitic to high-K basaltic scoriae and episodic paroxysmal eruptions and effusions of lava flows of the same compositions[1,2]. When all the subaerial geological record of Stromboli is considered, a much more variable range of eruptive styles, geochemical compositions and petrography are observed. Except for the Strombolicchio neck (200 ky), the subaerial part of Stromboli dates back to c. 85 ky BP and developed through six main eruptive epochs (Fig. 1), namely Paleostromboli I, II, III, Vancori, Neostromboli and Recent Stromboli[2,3]. The dominantly strombolian and effusive activity has occurred mostly from summit craters and subordinate lateral vents, with recurrent quiescence periods and erosional stages generally associated with caldera and lateral

[1]Dipartimento di Biologia Ecologia e Scienze della Terra, Università della Calabria, Via P. Bucci 15/B, 87036 Rende, CS, Italy. [2]Dipartimento di Scienze Biologiche Geologiche e Ambientali, Università di Catania, Corso Italia 56, 95128 Catania, Italy. [3]Institut for Earth System Sciences, Leibniz Universität Hannover, Callinstrasse 3, 30167 Hannover, Germany. [4]Dipartimento di Scienze della Terra e Geoambientali, Via Arabona 4, 70125 Bari, Italy. [5]IGAG-CNR, Via Mario Bianco 9, Milan, Italy. [6]Istituto Nazionale di Geofisica e Vulcanologia, Sezione Bologna, Bologna, Italy. [7]Dipartimento di Scienze Biologiche Geologiche e Ambientali, Università di Bologna, Via Zamboni 67, 95128 Bologna, Italy. ✉email: eugenio.nicotra@unical.it; federico.lucchi@unibo.it

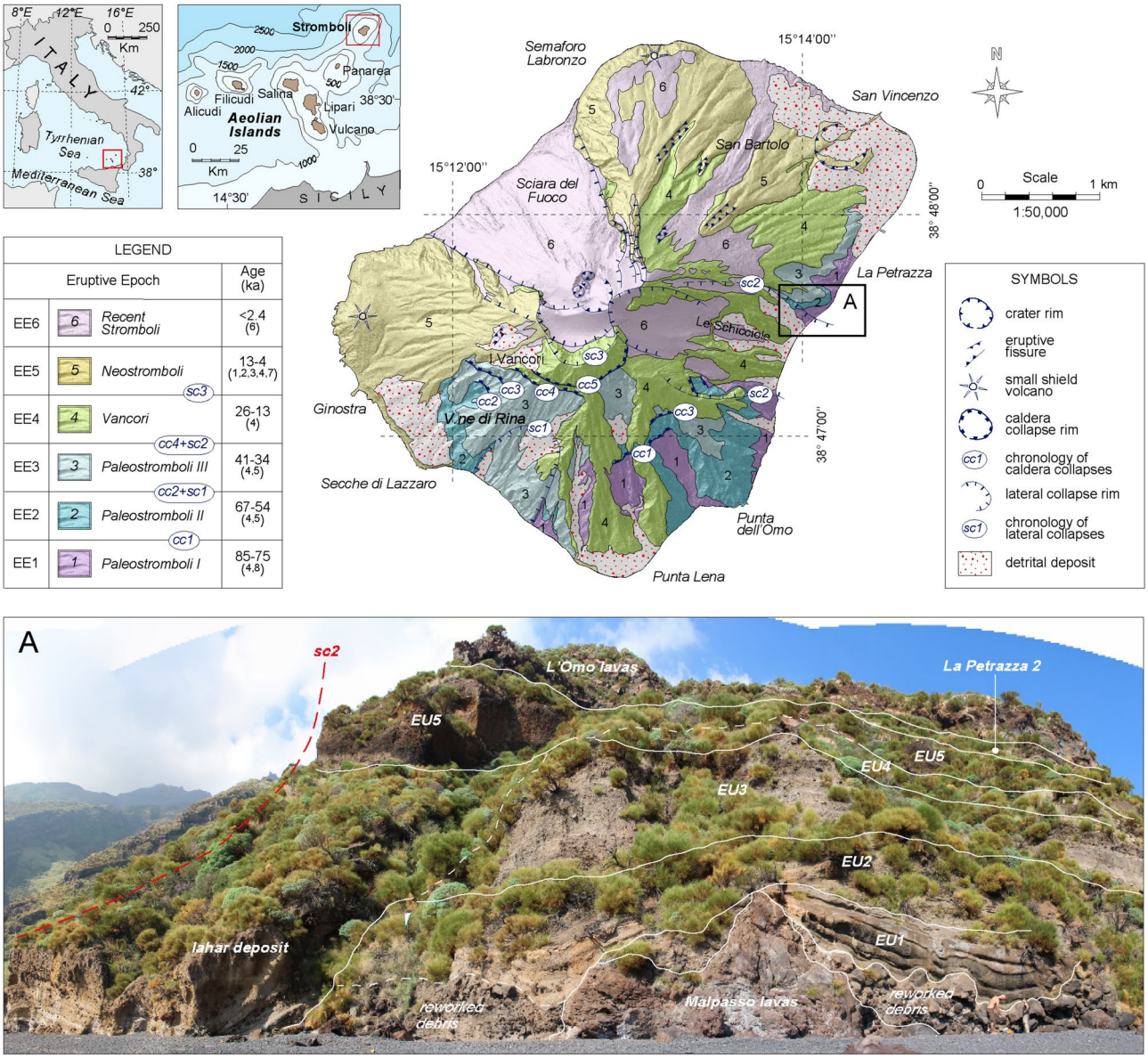

Fig. 1. Geological sketch map of the island of Stromboli from[2], with indication of areas of interest. In the inset, the position of Stromboli in the Aeolian archipelago and the southern Tyrrhenian Sea. (**A**) Outcrop site of La Petrazza, with the main general stratigraphic architecture of the PET sequence and the main boundaries of the reconstructed eruption units (EU1-EU5). The reworked debris material (or debris avalanche deposit) at the base of PET is visible, together with the lahar deposit that marks the occurrence of a major angular unconformity at the base of EU5. Towards the left the trace of the sc2 collapse is marked, which represents the latest major SE-dipping lateral collapse occurred in the area of Le Schicciole–Rina Grande.

collapses[2,4]. In particular, the volcano has been characterized by several sector collapses triggered by recurrent NE-SW-oriented dyke intrusions[2–5], which led to formation of the multi-stage collapse structures of Rina Grande (SW-dipping) and Sciara del Fuoco (NW-dipping). The eruptive epochs are associated with major changes in the chemical composition of erupted magmas from (dominant) basalts to (minor) trachytes relative to high-K calc-alkaline (HKCA) to shoshonitic (SHO) and potassic series[2,6]. Distinctive bimodal high- (HP) to low-porphyritic (LP) juvenile fragments, both with a shoshonitic to high-K calc-alkaline basaltic whole-rock composition, are erupted in the present-day activity (involving the last 1200 years) as the result of mingling processes between magmas spilled from different reservoirs at variable depths in a complex polybaric plumbing system[6–8]. Although the present-day activity of Stromboli is one of the most well-known and studied by volcanologists, less attention has been conversely given to its ancient eruptive activity.

The object of this paper is the Petrazza pyroclastic succession (PET; Fig. 1), emitted during the early stages of development of the Stromboli volcano, namely the Paleostromboli I epoch, between 85–67 ky BP[2,3]. Distal fallout lapilli and ash deposits correlated to PET have been reported on Panarea and Capo Milazzo peninsula[9–11] and in

the tephrostratigraphic records of the Ionian and Tyrrhenian seas and Monticchio lake[12], which have provided astronomically calibrated ages of 75.3 ky BP[13] and 77.1 ky BP[14] for PET. A general knowledge is available in the literature on this succession, which mostly corresponds with the so-called "La Petrazza Formation"[2], "Petrazza pyroclastic series"[3] and "Petrazza Tuffs"[15], but a detailed study is still lacking. We adopted a multidisciplinary approach that joined together stratigraphy and lithofacies analysis, whole rock and glass geochemistry, petrography and mineral chemistry, textural investigations on crystals and thermobarometric calculations with the aim of investigating the eruptive behaviour and pre- to syn-eruptive dynamics of the Petrazza pyroclastic succession, with a particular focus on the eruption triggers and the configuration of the corresponding magma plumbing system. By comparing the obtained results with what is known on the magmatic system driving the present-day activity, we infer conclusions on the possibility that large magnitude explosive eruptions similar to those of Petrazza should be considered as a potential eruptive scenario at Stromboli.

Results

Stratigraphy and lithofacies

PET is a 10–30 m-thick pyroclastic succession that crops out along the eastern and southern flanks of Stromboli (Fig. 1), although correlations are sometimes difficult due to the difficult accessibility of the outcrops and their preservation. Stratigraphically, it is located above the Malpasso lavas (Paleostromboli I, 85 ky) and is covered by the La Petrazza 2 scoriae (Paleostromboli I) and L'Omo lavas (Paleostromboli II, 64–54 ky BP). PET is composed of fallout deposits of massive breccia to agglomerate (ash-poor) or clast-supported lapilli alternating with ash-supported breccia deposits from pyroclastic density currents. These deposits include moderately to highly vesicular, light-grey to whitish pumices and dark-grey scoriae, with numerous banded juveniles and a number of irregular plastically deformed bombs. In its best field exposure near to La Petrazza site (Fig. 1A), PET rests above a thick heterolithologic and poorly sorted breccia (with hummocky surface) that could represent a debris avalanche deposit or reworked debris material. There, we have reconstructed a composite stratigraphic succession split into five eruption units (EU1-5) separated by local erosive and angular unconformities, paleosols and interlayered horizons of reworked debris (Fig. 2). In its mid-upper portion, the succession is also divided by a thick, massive to roughly stratified, heterolithologic yellowish lahar deposit (Fig. 1A), which is associated with a sharp angular unconformity between the EU4 and EU5. Some of the EUs are subdivided into different depositional units (e.g. $EU1_{A, B, C}$), representative of distinct eruptive pulses of fallout and pyroclastic density currents, based on lithofacies analysis and the occurrence of reworked beds and/or sharp grain size variations (following the approach of[16]). The different EUs and depositional units of PET, and their volcanological interpretation, are described in Table 1.

Whole rock and glass geochemistry

The whole rock compositions of products of PET eruptive cycle mostly belong to the high-K calc-alkaline series, with only glass compositions of some EUs that plot within the shoshonitic field (Fig. 3A; Supplementary Table S1). PET rocks are among the less K-enriched products in the whole Stromboli succession (Fig. 3A)[2]. Whole rock compositions vary from basalts to andesites (Fig. 3A), generally following a unique liquid line of descent (Fig. 3B), except for K_2O and (to a lesser extent) Na_2O, that present a higher variability between the different EUs (Table S1). The most basic compositions are those of the $EU1_A$ scoriae at the base of PET (Fig. 3C), showing an abrupt compositional change after the underlying Malpasso lavas, whereas pumice of the EU5 present the more K-rich compositions of the succession with dacite and latite to trachyte glass compositions (Fig. 3A). Mingled structures (banded juveniles) among these terms are present in the hand-sized samples of $EU1_B$, $EU2_A$ and EU3.

New data for the distal pumice lapilli found at Panarea tend to confirm the correlation with PET already proposed by[9–11], with glass compositions mirroring those of EU3 and indicating that the distal deposits are related to this eruption unit of PET (Fig. 3A-B). Whole rock data also confirmed the correlation with PET of the distal tephra layer (TM-21) in the Monticchio lake core[12].

Petrography and mineral chemistry

PET products are characterized by a quite constant and high porphyritic index (42–50 vol.%; Table 2), except for EU5 which is significantly less porphyritic (16 vol.%; Table 2). Most of the samples show a porphyritic seriate texture, with a high variability from poorly (20–40%) to moderately (40–60%) and highly vesicular (60–80%) and bubble size up to 3 mm. Groundmass varies from vacuolar hypocrystalline to cryptocrystalline (sometimes aphanitic) with variable amounts of glass, which turns from black-brownish (in the scoriae) to colourless (in the pumices), and microlites. Pumices and scoriae have the same paragenesis, similar to the typical mineral assemblage of Stromboli, except for the presence of amphibole in some units (Table 2). Except for EU5, all the analyzed rocks have large (up to 2 mm) glomerocrysts mostly made up by clinopyroxenes ($\pm$ Pl $\pm$ Ol $\pm$ Opx $\pm$ Amph). The PET pumices collected at Panarea present a similar mineralogical paragenesis, amphibole included, although with a higher degree of alteration.

Plagioclase is the dominant mineralogical phase. Crystals are large (up to 3 mm), mainly euhedral (except in EU5 where mainly crystal fragments are visible), always twinned and zoned, with very rare sericitic alteration (especially in EU5). They show an extremely wide compositional range [An_{45-86}; Anorthite = (100*(Ca + Na)/Ca) in mol%] both at core and rim positions of the crystals (see the next chapter for further details). Clinopyroxenes vary between diopside and augite (Table S2), rarely presenting "hourglass" zoning, and show a slight variation of Mg number [Mg# = 100 Mg/(Mg + Fe^{2+}) in mol%] between the core (Mg# 0.73–0.87) and the rim (Mg# 0.68–0.88) of the crystals. Orthopyroxenes occur as phenocrysts (< 1–10 vol.%) or as envelope of clinopyroxene crystal cores, showing a smaller compositional range between the cores (Mg# 0.69–0.74) and the rims (Mg# 0.71–0.76). Olivine is present as fresh euhedral-to-subhedral phenocrysts of small size, with a narrow compositional range and high forsterite content [Fo_{82-89}; Fo = 100*Mg/(Ca + Fe + Mg) in mol%].

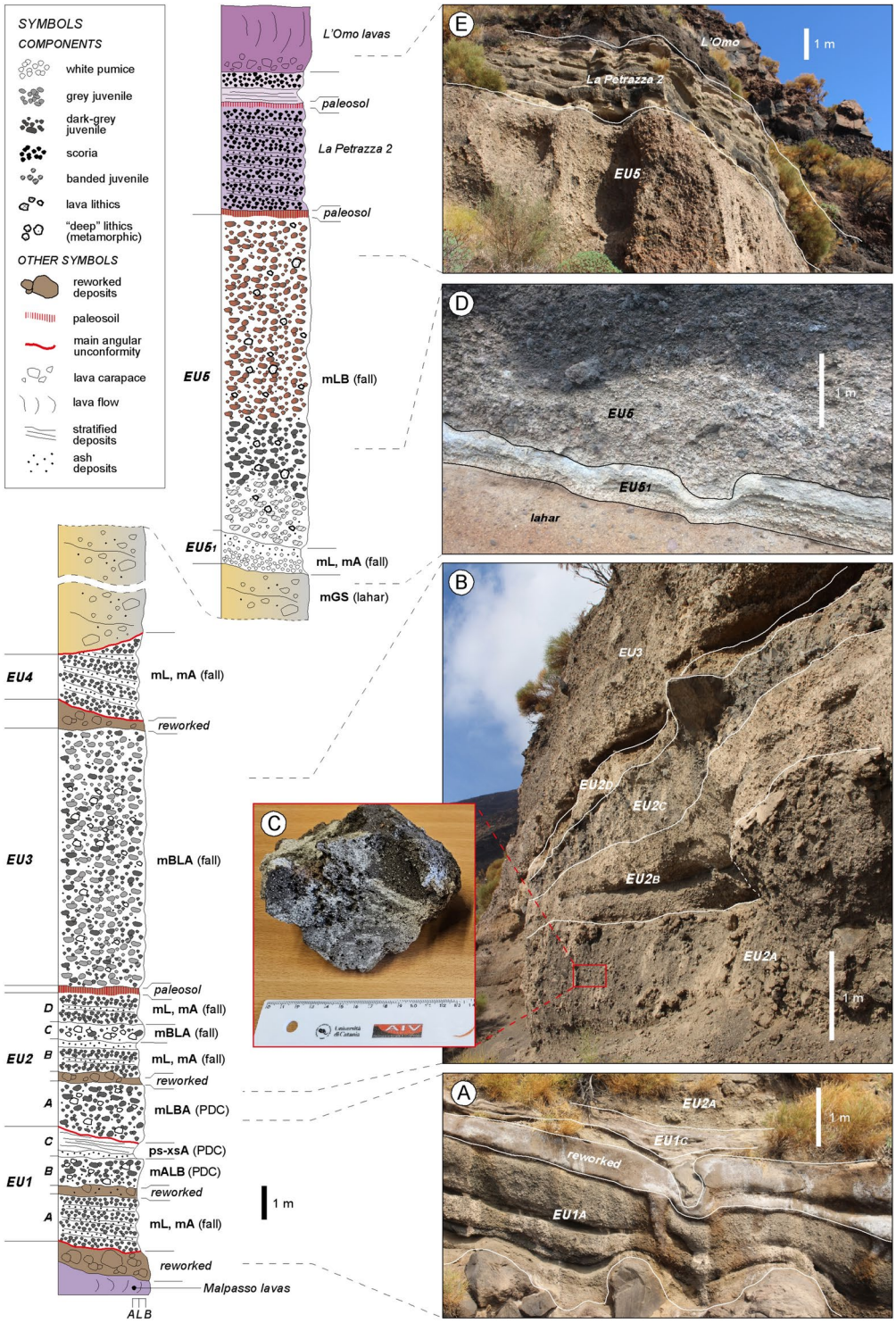

Fig. 2. Generalized stratigraphic succession of PET in the main outcrop site of La Petrazza, showing the subdivision into different eruption units (EU1-EU5), and their further subdivision into depositional units (e.g. $EU1_{A\text{-}C}$) representing different eruptive pulses. Each eruption unit (and depositional unit) is characterized in terms of lithofacies (see Table 1 for explanation) and volcanological interpretation (PDC = pyroclastic density currents, fall, lahar). Outcrop photographs (**A**–**E**) of the different portions of PET are provided (see Table 1 for details of the distinct eruption units and depositional units). A banded juvenile clast related to unit $EU2_A$ is shown in C.

Eruption unit	Depositional unit	Lithofacies	Products	Components	Interpretation
EU5	EU5B	mLB	Breccia deposit of clast-supported (ash-poor) lapilli and bombs (up to 50 cm Ø) and lithic blocks, with an enrichment of lithic fragments in the upper part, together with grey bombs. Distinctive flattened dark-grey bombs are visible in the basal part of the unit. The basal portion is whitish due to wide hydrothermal alteration of the primary pyroclasts. Thickness variable from 9 metres in the key outcrop to 20 metres in southern Stromboli with a mantle-bedding attitude	Dark-grey juveniles dominantly characterized by an orange patina due to oxidation (particularly in the mid-upper portion), variable content of heterolithologic (lava to metamorphic) lithics (up to 30%)	Mantle-bedding, scarce ash content and clast-supported fabric suggest direct fallout deposition from an eruptive column
	EU5A	mL, mA	30-40 cm-thick bed of angular to sub-angular lapilli (up to 6 cm Ø) with distinctive charcoal fragments, gradually upwards passing to a 30 cm bed of massive ash and scarse lapilli	Whitish to grey, and banded pumice	Direct fallout from an eruptive column of variable height
		mGS	Up to 6 m thick massive to roughly stratified deposit of heterolithologic granules to cobbles supported in a yellowish sand matrix	Lava to scoria fragments	Deposition from lahars
EU4		mL, mA	Metre-thick alternation of beds (10-20 cm thick) of well-sorted, angular lapilli separated by massive ash	Grey juveniles	Direct fallout from an eruptive column of variable height
EU3		mBLA	Massive breccia deposit (up to 10 m thick) of ashsupported lapilli and bombs. The deposit is ashpoor, in places with an open framework fabric and localized enrichment of clast-supported (coarse-grained) clasts	Grey to dark grey juveniles, banded juveniles, lava to metamorphic lithics	Scarce ash content and localized clastsupported fabric suggest direct fallout deposition from an eruptive column in a proximal occurrence. Alternatively, rapid deposition from a PDC at high concentration derived from column collapse cannot be completely discounted
EU2	EU2D	mL, mA	Two fall beds (each 20 cm thick) of well-sorted, angular lapilli separated by massive ash	Grey juveniles, lithics	Direct fallout from an eruptive column of variable height
	EU2C	mBLA	Massive breccia deposit (30 cm thick) with angular lapilli and abundant lithic blocks (up to 50 cm Ø) and minor ash	Dark-grey lava lithics (up to 60%), grey juveniles	Angular fragments, abundant lithics and scarce ash content suggest direct fallout deposition from an eruptive column in a proximal occurrence
	EU2B	mL, mA	Two beds (30 and 45 cm thick) of well-sorted, angular lapilli separated by irregular beds of massive ash and sparse lapilli	Grey juveniles, lava lithics (up to 40%)	Direct fallout from an eruptive column of variable height
	EU2A	mLBA	Breccia deposit (1,5 m thick, variable) of massive, ash-supported lapilli and bombs/blocks with a distinctive content of cauliflower bombs (up to 60 cm Ø) particularly in the mid-upper portion of the deposit	Grey to dark-grey juveniles (banded cauliflower bombs), lithics (up to 30%)	Poor sorting, abundant ash and massive appearance suggest rapid deposition from a PDC at high concentration derived from column collapse
EU1	EU1C	psA, xsA, mA	Planar to cross stratified ash deposits (80 cm thick, variable), with a layer of indurated massive ash at the base	Grey to dark-grey juveniles, lava lithics	Planar to cross stratification indicates deposition from diluted and turbulent PDCs dominated by traction processes. Massive ash suggests gentle settling from a diluted ash cloud with a negligible lateral transport
	EU1B	mALB	Breccia deposit (1 m thick, variable) of poorly sorted, ash-supported lapilli and bombs with a distinctive enrichment of cauliflower bombs (up to 25 cm Ø) at the top	Grey to dark-grey juveniles (banded cauliflower bombs), lava lithics	Poor sorting, abundant ash and massive appearance suggest rapid deposition from a PDC at high concentration derived from column collapse
	EU1A	mL, mA	M-thick sequence of distinct beds of well-sorted, angular lapilli and ash which which mantles the underlying deposits	Dark-grey scoriae, scarce lava lithics	Direct fallout from an eruptive column of variable height

Table 1. Lithofacies codes, description of the products, main components and volcanological interpretation of the different Eruption Units (EUs) recognized in the Petrazza succession. Some of the EUs have been subdivided into different depositional units (A–D) based on their lithofacies and the occurrence of reworked beds and/or sharp grain size variations (following the approach by Lucchi, 2013). The first letters of the lithofacies code indicate the general appearance of the deposit (m = massive, ps = planar stratified, xs = cross-stratified, is = intermittently stratified, etc.) and the capital letters indicate the grain size (A = ash, L = lapilli, B = Blocks/Bombs). The different EUs are interpreted in terms of deposits from fallout and/or pyroclastic density currents and reworked volcaniclastic deposits (and lahars).

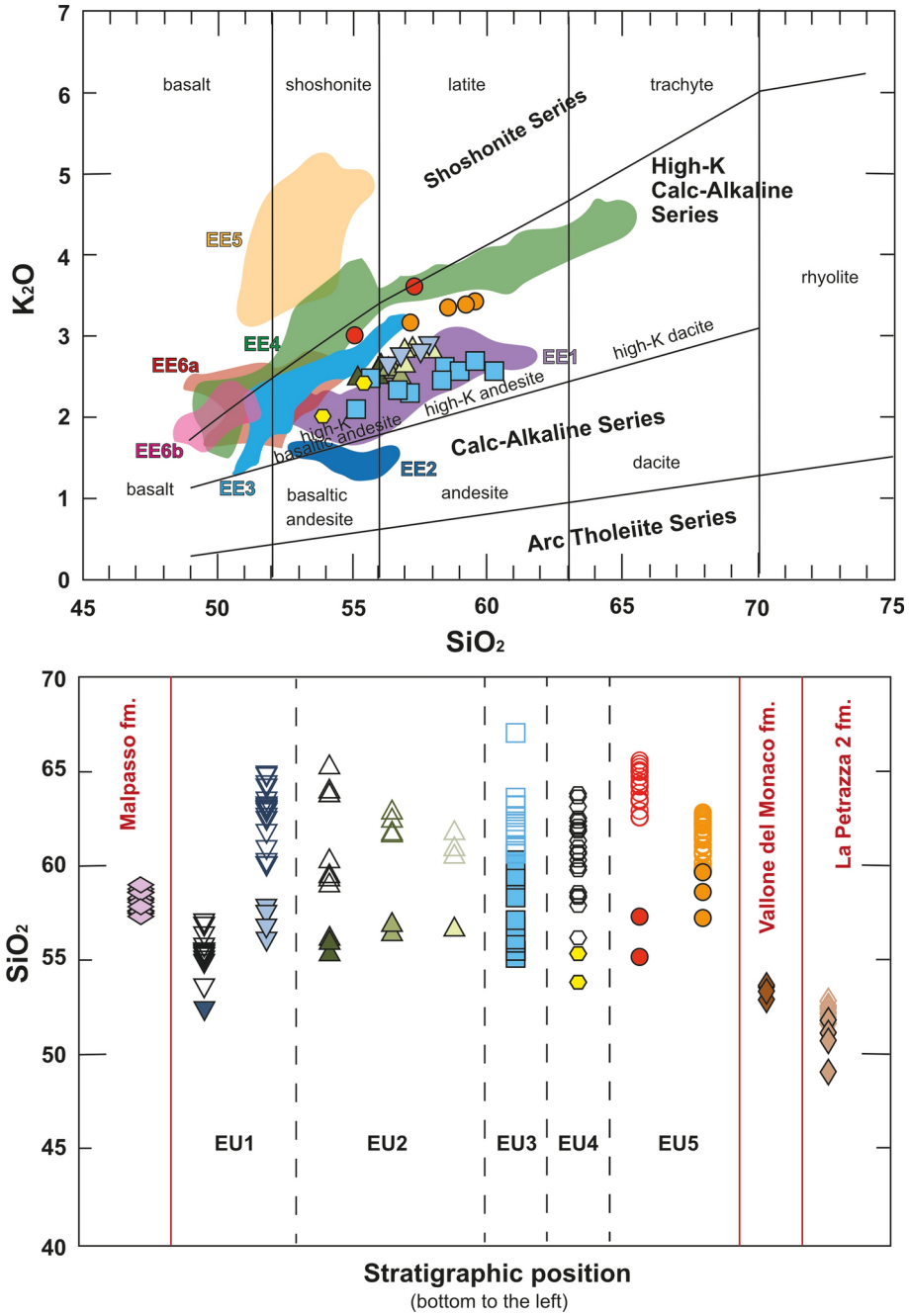

Fig. 3. Whole rock and glass compositions for the collected samples of PET. (**A**) SiO_2 vs. K_2O diagram of the considered succession (only whole rock). EE = Eruptive Epochs (as defined by[48]) for Stromboli island[2]: EE1: Paleostromboli, EE2: Paleostromboli II; EE3: Paleostromboli III; EE4: Vancori; EE5: Neostromboli; EE6a: Pizzo, San Bartolo; EE6b: Present-day. (**B**) CaO/Al_2O_3 vs. FeO_{tot}/MgO diagram for the analyzed glass of collected rocks. Most of compositions lie on the same liquid line of descent, included the pumice lapilli found at Panarea (black crosses). (**C**) SiO_2 composition behavior with respect to the stratigraphic position (bottom of the sequence on the left). The underlying Malpasso formation (fm.) and the overlying Vallone del Monaco and La Petrazza 2 formations are included for comparison.

Amphibole phenocrysts of medium-to-large size mainly occur in EU3 unit (up to 12 vol.%; Table 2), whereas they are present as scarce (< 5 vol%) microphenocrysts in EU4-EU5 and are absent in unit $EU1_A$ and rare (< 1 vol%) micro-phenocrysts in units $EU1_{B\text{-}C}$ and EU2 (< 3 vol.%). The presence of amphibole crystals predominantly in EU3, as well as in the distal pumices at Panarea, is another element that supports this correlation. Amphibole also occur in glomerocrysts of units $EU1_B$, $EU2_A$ and EU4, and they were observed within gabbroic cumulate nodules in cognate lithic fragments[17,18]. Amphibole phenocrysts in EU3 (but also of EU4-5) are clear and euhedral, with linear and straight edges and no opaque rims typical of amphiboles (Fig. 4),

Eruption unit	Sample	Pl [vol%]	CPx [vol%]	OPx [vol%]	Ol [vol%]	Amp [vol%]	Opq [vol%]	P.I.	P.I.AVG
$EU1_A$	ST19-16	22	16	-	2	–	<1	40	40
$EU1_B$	ST19-7a	24	12	1	1	–	2	40	43
	ST19-7abis	20	12	5	2	–	1	40	
	ST19-7b	23	13	9	4	< 1	2	50	
	ST19-7c	16	8	8	7	< 1	1	40	
$EU2_A$	ST19-8	20	9	10	10	< 1	2	50	50
	ST19-10	20	13	9	8	< 1	2	50	
	ST19-23	26	16	5	3	–	2	50	
$EU2_B$	ST19-24	23	16	5	5	–	2	50	45
	ST19-25	18	12	6	2	–	2	40	
$EU2_C$	ST19-26	23	14	7	2	<1	-	45	45
	ST19-11	23	9	8	3	8	2	50	
	ST19-12S	15	10	8	5	10	3	50	
	ST19-12C	17	2	6	2	12	1	40	
	ST19-13	24	12	6	3	12	3	60	
	ST19-14	16	8	2	–	12	2	40	
	ST19-15	20	13	5	3	8	3	50	
	ST19-27a	16	9	6	3	6	–	40	
	ST19-27b	15	9	6	4	5	1	40	
	ST19-27c	16	12	2	3	6	1	40	
EU3	ST19-9	25	13	8	3	<1	2	50	46
EU4	ST19-30	16	11	4	2	6	1	40	45
	ST19-17	23	15	8	3	1	2	50	
EU5	ST19-34	7	1	–	–	4	–	12	16
	ST19-35	7	6	–	1	5	1	20	
	ST19-31	6	3	–	-	5	-	15	
Crystal size		up to 3 mm	up to 2 mm	up to 0.8 mm	up to 0.7 mm	up to 2,6 mm	–		

Table 2. Petrography of PET. Pl = plagioclase; CPx = clinopyroxene; OPx = orthopyroxene; Ol = olivine; Amp = amphibole; Opq = opaque crystals; PI = Porphyritic Index.

suggesting they are in equilibrium with the surrounding magma. Only amphiboles in EU3 show opaque rims (Fig. 4c) generally associated to rapid transitions to disequilibrium conditions[19]. Amphiboles show a wide range of Mg# both in the cores (0.63–0.71) and the rims (0.64–0.71; Supplementary Table S3). Overall, they vary from Mg-hastingsite to Mg-hornblende in composition, with low contents of TiO_2 (1.7–2.9 wt.%) and K_2O (0.8–1.2 wt.%), and a wide compositional range for Al_2O_3 (7.5–13.4 wt.%). Small micro-fragments of calcic amphiboles were recognized also within the distal pumices of PET on Panarea[9,11].

Textural and compositional features of plagioclase crystals

Four main plagioclase textures, also coexisting in the same crystals, have been distinguished within the PET products (Fig. 5; Table S4): (1) oscillatory-zoned crystals; (2) crystals with concentric envelops of melt inclusions; (3) resorbed crystals; (4) envelopes of resorption.

Oscillatory zoned plagioclases mostly show small and "normal" oscillations of the An content ($< \Delta An_8$) at negligible variations of FeO and with no peculiar optical textures (Fig. 5A, B), whereas "reverse" oscillations occur only in a few samples of $EU1_B$ and EU3.Two different amplitudes of An-content oscillation ($\Delta An_{1\text{-}4}$ and $\Delta An_{5\text{-}8}$) with FeO oscillation < 0.4 wt.% are found (Fig. 5A). Along the stratigraphy of PET, oscillatory-zoned plagioclases increase from EU1 to EU2 (13% and 34%, respectively), and then upwards lower in EU3-EU4-EU5 (17–24%, Fig. 6).

Oscillatory zoning in some plagioclases is interrupted by one or more envelops of μm-sized melt inclusions (MI) aligned along crystallographic directions (Fig. 5C, D; Table S4). Plagioclases commonly present up to two concentric layers of MIs in $EU1_A$, $EU2_{A\text{-}B}$, EU5, three layers in units $EU2_C$ and EU3 and 4 layers in one plagioclase of $EU1_B$. In correspondence of these envelopes compositional profiles present an increase of the anorthite content up to ΔAn_{18} at constant FeO in $EU1_B$, $EU2_A$, $EU2_C$ (Fig. 5C, D; Table S4). This texture is the most abundant in PET (13–49%; Fig. 6), with three peaks of abundance in units $EU1_{A\text{-}B}$and $EU2_B$.

Plagioclases may be characterized by areas of resorption/dissolution in the cores (Resorbed cores, RC) or across the whole crystal (Table S4), mainly due to disequilibrium conditions with the surrounding magma. They are associated with a decreasing trend or a sudden drop of the anorthite content (up to ΔAn_{20}) at constant FeO content (Fig. 5E, F). RC textures can be associated to oscillatory zoning or envelops of resorption at rim positions (e.g., in $EU2_A$ and $EU2_B$ respectively). Resorbed-core plagioclases vary from 19 to 36% in EU1 and EU4, with a considerable peak of 45% in EU5 where this texture is dominant (Fig. 6) and most of the cores are almost totally dissolved.

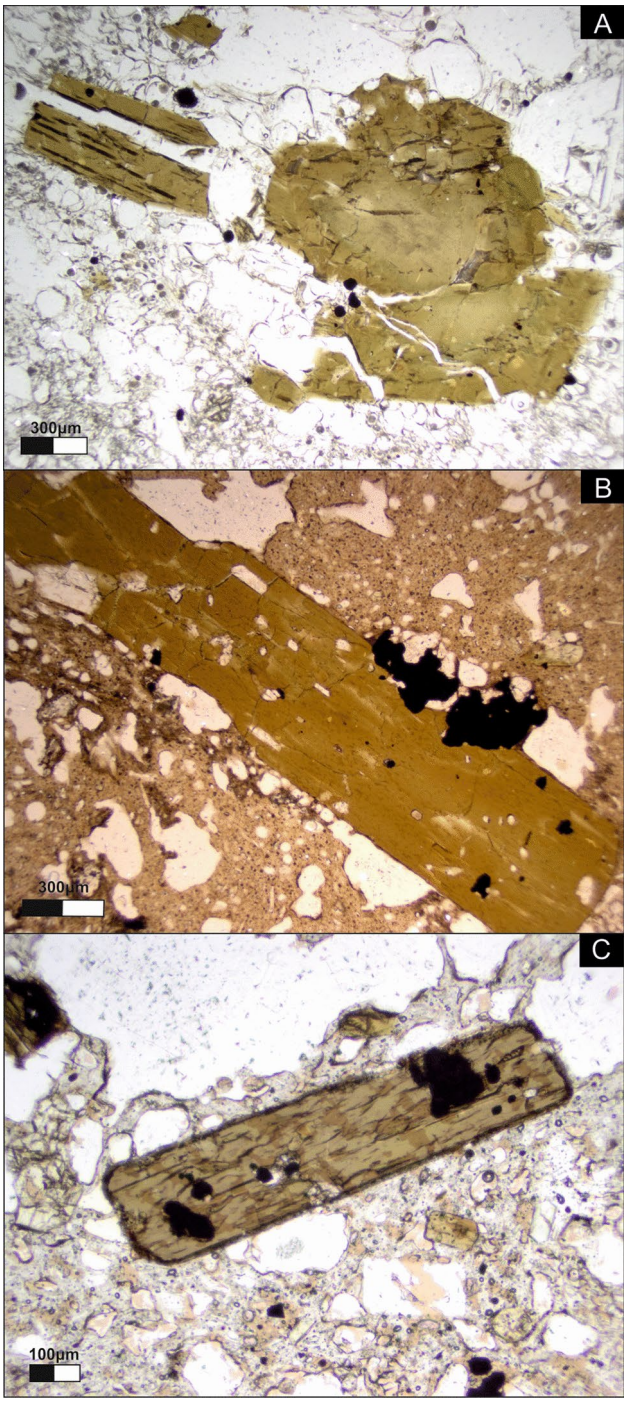

Fig. 4. Amphibole crystals in the PET succession. Amphiboles in (**A**, **B**; ST19-14 and ST19-35 samples) belong respectively to the EU3 and EU5, and do not present opaque reaction rims, as instead shown by the crystal in (**C**), belonging to EU3 (ST19-13 sample).

Plagioclases with envelopes of resorption (ER) are characterized by the development of > 30 µm-thick bands of coarse-to- dusty sieve-textures in rim positions (Fig. 5A, B). They are aligned along the crystal growth planes and generally followed by a 3–15 µm-thick oscillatory zoning layer (e.g. in $EU2_A$; Table S4). The most pronounced envelopes of resorption are recognized in $EU2_A$ and EU3 (Fig. 5A, B). This texture is characterized by a concordant increase of An (up to ΔAn_8) and FeO contents (up to 2 wt.%) in correspondence of the MI layer (Fig. 5a, b). Crystals with envelopes of resorption are the least frequent in PET (from 2 to 19%), and the highest values are notably recorded in $EU1_B$, $EU2_A$, EU3 and EU5.

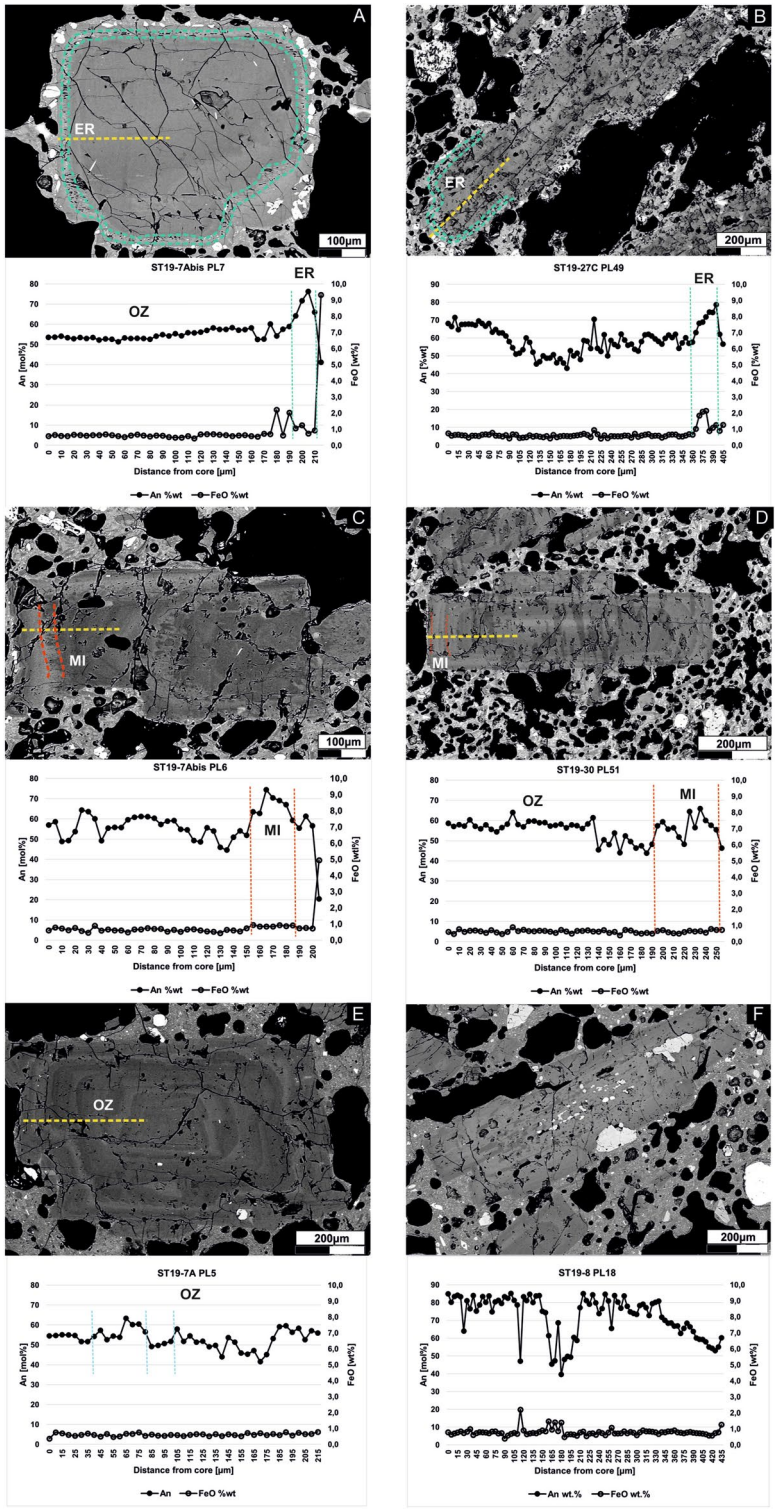

Fig. 5. Back-scattered electron images acquired through Scanning Electron Microscope (SEM) and compositional core-to-rim profile of selected plagioclase crystals of PET. (**A**, plagioclase from $EU1_B$; **B** from EU3) Plagioclase with Oscillatory Zoning (OZ) pattern for most of the crystal and an Enveloped Rim (ER) texture in outer position characterized by the development of > 30 µm-thick bands of coarse to dusty sieve-textures and an increase of ΔAn_{20} at negligible FeO variations; (**C**, plagioclase from $EU1_B$; **D** from EU4) Oscillatory zoning is interrupted by layers of Melt Inclusions (MI), aligned along crystallographic directions. In correspondence of the melt inclusions layers an increase of $\Delta An_{20\text{-}25}$ is observed, at no variations for FeO. (**E**, plagioclase from $EU1_B$; **F**, $EU2_A$)) Plagioclase with Resorbed Core (RC) texture, with a typical rounded core marked by a ΔAn_{20-30} decrease at fairly constant FeO contents.

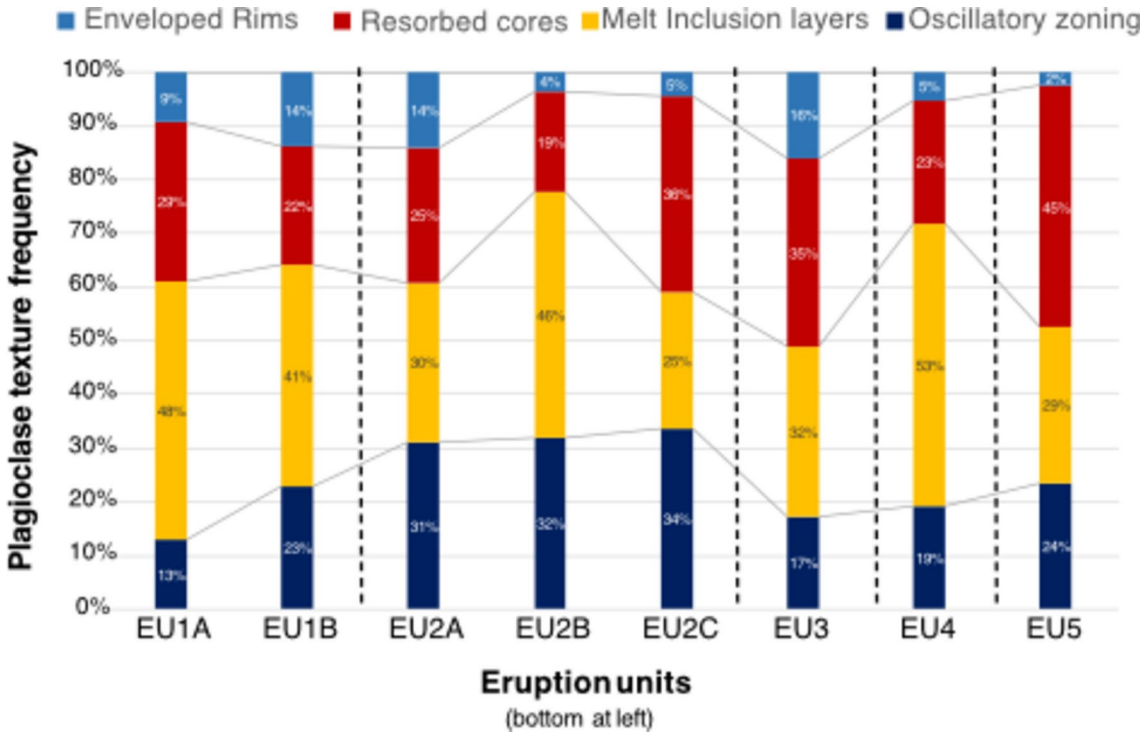

Fig. 6. Frequency for each texture found in more than 3500 plagioclase phenocrysts (> 500 μm) in the rock samples of each eruption unit. Only entire (no fragments) of crystals have been counted. Antecrysts and xenocrysts are not included in the total counting (cf. Methods section).

Thermobarometric calculations

In order to obtain pressures of crystallization for the PET magmas, we used the geothermobarometer of[20] on 33 amphibole crystals (Table 3) and the thermobarometer of[21] on 24 clinopyroxene crystals. In general, thermobarometric models cannot be applied when the surrounding magma experiences mixing processes[19,22,23]. In this view, we consider the general assumption that there was a very fast magma recharge within the PET feeding system, allowing minerals to preserve equilibrium conditions in the form of homogeneous phenocrysts or intra-crystal domains. If so, also in the case of the banded juveniles within PET, a substantial chemical mixing is avoided. According to[20], single-amphibole thermobarometry can only be applied to homogeneous crystals or intra-crystal domains (recording an equilibrium "steady-state" condition of magmatic crystallization), conditions identified within the amphibole phenocrysts in units $EU1_B$, $EU2_A$, EU3 and EU5. Among other thermobarometers, the advantage of using this method is that it relies in low T, oxygen fugacity (fO_2), volatile content in the melt (H_2O_{melt}) uncertainties (i.e. ± 24 °C, 0.4 log units and 14%, respectively). In particular, P uncertainty is rather low and relative (i.e. 12%). It is used to countercheck the validity of the method by comparison of the P standard deviation of homogeneous domains, that should be lower than 12%[20]. Conversely, the clinopyroxene-only thermobarometer[21] gave reliable results only for units $EU1_{A-B}$, $EU2_{A-C}$, EU_3 (Table 3).

Overall, a polybaric magma plumbing system is depicted for PET (Fig. 7; Table 3). More in detail, the amphibole thermobarometry mostly indicate crystallization of PET magmas at crustal conditions (130–580 MPa, 5–22 km depth) and temperatures of 810–960 °C. The basal units of PET ($EU1_B$ and $EU2_A$) show P–T ranges of 210–400 MPa (8–15 km depth) and 880–950 °C. The entire range is present in the EU3 magma. All the amphiboles in these units ($EU1_B$, $EU2_A$ and EU_3) show large fO_2 (ΔNNO, i.e. $\log fO_2 - \log fO_2$ at the Ni-NiO buffer) = 0.6–3.6) and H_2O_{melt} (4.0–6.7 wt.%) variations and are mostly characterized by normally and inversely zoned phenocrysts. This suggests a very dynamic environment characterized by convection and mixing processes in different magmatic zones in the pressure interval of 133–422 MPa at depths of 5–16 km (Fig. 7; Table 3). By contrast, the amphiboles in the upper unit of PET (EU5) are not zoned and indicate limited P–T-H_2Omelt-fO_2 crystallization conditions at pressures of 300–320 MPa (~ 12 km depth), temperatures of 916–920 °C, H_2Omelt of 5.1–5.3 wt.%, and oxygen fugacity (ΔNNO) of 1.7–2.1.

The clinopyroxene thermobarometry of[21] resulted in pressures of crystallization between 100 and 370 MPa, at depths of 3.7–13.7 km (considering an average crustal density of 2.7 g/cm^3[23] (Table 3). Following the stratigraphic order, the lowermost $EU1_{A-B}$ units, where only dark scoriaceous and highly-porphyritic lapilli are emitted, present the lowermost range of depths of crystallization of the entire sequence (3.8–5.3 km, av. 4.6 km; Table 3). Furthermore, except for the single highest value of 7.5 km (194 MPa) is not considered, most of the considered clinopyroxene crystallize in a very narrow range of crystallization (100–140 MPa, or 3.8–5.3 km; Table 3). Clinopyroxenes of $EU2_{A-C}$ highlight a deepening of the depth of crystallization through time. In particular, except for one crystal giving 110 MPa, the main crystallization depths vary from 150 to 320 MPa, with an average value of 190 MPa for $EU2_A$ and 225 MPa for $EU2_C$ (7.1 and 8.7 km, respectively; Table 3). Similar

La Petrazza Fm. (77-75ka)—Paleostromboli I												
Clinopyroxene[21]							Amphibole[20]					
Eruptive Unit	Sample	P [MPa]	T [°C]	P_{avg} [MPa]	Depth [km]	$Depth_{avg}$ [km]	Eruptive Unit	Sample	P [MPa]	T [°C]	P_{avg} [MPa]	Depth [km]	$Depth_{avg}$ [km]
EU1A	ST19-16_Cpx1r	114.4	1136.6	118.7	4.4	4.6	EU1B	ST19-7Abis_Amp1$_{mantle}$	397.7	947.8	309.7	15.3	11.9
	ST19-16_Cpx2i	138.1	1138.1		5.3			ST19-7Abis_Amp1$_{rim}$	291.1	919.1		11.2	
	ST19-16_Cpx3i	124.1	1181.5		4.8			ST19-7B_Amp1$_{homo}$	240.4	912.6		9.3	
	ST19-16_Cpx3r	98.1	1135.7		3.8		EU2A	ST19-08_Amp1_1$_{core}$	207.7	875.5	216.4	8.0	8.3
EU1B	ST19-7A_Cpx2i	115.0	1123.6	142.9	4.4	5.5		ST19-08_Amp1_2$_{homo}$	225.1	896.2		8.7	
	ST19-7Abis_Cpx2r	194.4	1184.7		7.5		EU3	ST19-11_Amp6$_{mantle}$	180.0	870.9	252.7	7.2	9.7
	ST19-7B_Cpx01c	119.2	1115.3		4.6			ST19-11_Amp5$_{somezone}$	174.3	858.3		6.7	
EU2A	ST19-08_Cpx01c	168.5	1154.4	204.6	6.5	7.9		ST19-11_Amp8$_{homo}$	170.8	856.7		6.6	
	ST19-08_Cpx01i	160.9	1147.5		6.2			ST19-12_Amp8$_{homo}$	370.1	958.6		14.3	
	ST19-08_Cpx01r	109.4	1140.5		4.2			ST19-12_Amp9	579.9	955.4		22.3	
	ST19-08_Cpx0c	315.6	1179.6		12.2			ST19-12_Amp11$_{somezone}$	249.5	905.9		9.6	
	ST19-08_Cpx0i	232.0	1181.0		8.9			ST19-12_Amp11$_{mantle}$	422.1	938.8		16.3	
	ST19-10_Cpx2i	194.6	1147.4		7.5			ST19-13_Amp12$_{core}$	152.1	829.1		5.9	
	ST19-10_Cpx2r	251.3	1141.8		9.7			ST19-13_Amp12$_{mantle}$	133.2	813.1		5.1	
EU2B	ST19-24_Cpx2i	105.7	1109.8	161.9	4.1	6.2		ST19-13_Amp13$_{homo}$	272.6	910.1		10.5	
	ST19-24_Cpx2r	108.0	1103.6		4.2			ST19-13_Amp14$_{core}$	307.3	913.8		11.8	
	ST19-24_Cpx1c	189.8	1164.4		7.3			ST19-13_Amp14$_{mantle}$	237.5	896.5		9.1	
	ST19-24_Cpx1r	263.6	1176.3		10.2			ST19-13_Amp14$_{rim}$	209.1	887.0		8.1	
	ST19-24_Cpx2c	179.1	1165.5		6.9			ST19-14_Amp4$_{homo}$	231.9	896.1		8.9	
	ST19-24_Cpx2i	141.8	1160.8		5.5			ST19-14_Amp2$_{homo}$	191.6	875.4		7.4	
	ST19-24_Cpx2r	145.4	1167.6		5.6			ST19-15_Amp16$_{homo}$	196.7	872.2		7.6	
EU2C	ST19-26_Cpx2c	195.1	1168.5	225.3	7.5	8.7		ST19-15_Amp15$_{homo}$	162.0	846.9		6.2	
	ST19-26_Cpx2r	255.5	1184.4		9.8			ST19-27a_Amp3$_{core}$	153.6	842.5		5.9	
EU3	ST19-11_Cpx_1c	200.3	1182.1	199.3	7.7	7.7		ST19-27a_Amp1$_{core}$	165.4	857.5		6.4	
	ST19-11_Cpx_2c	152.4	1178.8		5.9			ST19-27a_Amp1$_{mantle}$	284.2	905.0		10.9	
	ST19-11_Cpx_2i	157.0	1166.1		6.0			ST19-27a_Amp2	251.7	906.8		9.7	
	ST19-11_Cpx_3c	298.3	1199.2		11.5			ST19-27c_Amp2$_{core}$	287.4	921.2		11.1	
	ST19-11_Cpx_3i	363.6	1207.3		14.0			ST19-27c_Amp3$_{core}$	265.4	915.5		10.2	
	ST19-14_Cpx_3i	175.8	1132.9		6.8			ST19-27c_Amp3$_{rim}$	243.4	910.1		9.4	
	ST19-14_Cpx_3r	228.6	1121.5		8.8			ST19-27c_Amp1$_{mantle}$	293.3	919.3		11.3	
	ST19-27a_Cpx1c	309.3	1169.1		11.9			ST19-27c_Amp1$_{rim}$	386.2	937.5		14.9	
	ST19-27a_Cpx1i	136.9	1164.6		5.3		EU5	ST19-35Amp5$_{homo}$	319.3	916.4	316.0	12.3	12.2
	ST19-27a_Cpx3c	108.2	1112.6		4.2			ST19-35Amp2$_{homo}$	320.8	918.7		12.4	
	ST19-27a_Cpx1c	140.1	1140.6		5.4			ST19-35Amp1$_{homo}$	305.3	918.1		11.8	
	ST19-27a_Cpx1i	233.9	1168.8		9.0			ST19-28Amp7$_{homo}$	318.6	920.1		12.3	
	ST19-27a_Cpx1r	170.2	1117.3		6.6								
	ST19-27b_Cpx1i	132.7	1139.3		5.1								
	ST19-27b_Cpx1r	168.7	1087.9		6.5								
	ST19-27b_Cpx2c	118.1	1162.5		4.5								
	ST19-27b_Cpx3c	204.6	1180.2		7.9								
	ST19-27b_Cpx3i	289.4	1192.8		11.1								

Table 3. Amp-TB2.xlsx[20] results for the amphibole and Cpx-barometry[21] phenocrysts in the units of PET. Uncertainties are reported as σ values of the multiple-profile conditions. P-depth conversion is calculated using a crust density of 2650 kg/m^3.

values are given by the pyroxene barometry for EU3, resulting between 108 and 364 MPa (4–14 km of depth) with a mean value of 200 MPa (7.7 km of depth).

Discussion

The combination of stratigraphy and volcanological interpretation with the petrochemical and thermobarometric investigation shows that PET has unique characteristics compared to the eruptive style that characterizes Stromboli during the present-day activity. This is why it is fundamental and urgent to define the trigger mechanisms and eruption style of this volcano. Hereafter we discuss the main features of PET eruptive behaviour, the geometry of its magma plumbing system at that time, the pre- and syn-eruptive dynamics and the possible eruption triggers. The results are then compared with those of the present-day activity of Stromboli to highlight what information is useful for defining eruptive scenarios in the context of hazard assessment.

Eruptive behavior

The thick accumulations of pyroclastic products (EU1-EU5) of PET, spaced out by erosional surfaces, angular unconformities and reworked deposits suggests a prolonged eruptive cycle lasting decades to hundreds of years around 75–77 ky BP. This period was characterized by alternating moderate to high-energy explosive eruptions and quiescent periods of different duration. The paleosol at base of EU3 records a prolonged period of subaerial exposure and pedogenesis, whereas the sharp angular unconformity separating EU4 and EU5, associated with thick lahar deposits, is a major unconformity within the succession recording massive erosion and reworking processes associated to a large-scale re-organization of the volcanic system. The alternation of fallout beds and pyroclastic density current deposits (recorded in different depositional units) throughout most of the PET eruptive cycle indicates intermittent eruptive dynamics with the rapid succession of phases of sustained column alternating with pyroclastic density currents from an eruptive plume with a transitional behavior between the buoyant and collapse regimes. This is typical of Vulcanian to sub-Plinian eruptions occurring when overpressure exceeds the resisting viscous forces and/or local lithostatic stress, although these styles of activity are unusual in low viscous magmatic systems like Stromboli. Distinct lithic-rich breccia units are found as the evidence of phases of vent-opening or enlargement of the crater area, which is compatible with the defined eruptive behaviour.

Calculation of the eruptive parameters (volume and mass discharge rate) is complicated by the fact of not having a considerable number of outcrops available from which to obtain data on the thickness and grain size of the deposit. On the other hand, we have demonstrated that EU3, in particular, is a fallout able to disperse distal ash and lapilli recognized up to 250 km from the vent (e.g., Panarea, Capo Milazzo, Lago Grande di Monticchio). Considering their similar thickness and grain size in proximal areas, EU5 must also have had a similar dispersion of deposits, even if it is not possible to univocally recognize the corresponding distal deposits. Assuming that the distal deposits are all correlated to EU3, as previously hypothesized on the basis of the similar composition of the glasses and presence of amphibole crystals, the range of the bulk volume of the erupted material can be roughly assessed using the method of[24], which is based on geometric assumptions and mathematical manipulations of thickness and distance using only two points. The method yields for EU3 a bulk volume comprised between 2.5 km^3 and 10 km^3, which correspond to a DRE of 1 km^3 and 4 km^3, respectively. These values may be roughly halved if we consider the distal deposits equally composed of EU3 and EU5 deposits, which would be reasonable if we consider that these two eruption units have comparable thicknesses in proximal areas. Volumes of this type fall within the range typically defined for Plinian eruptions, consistent with the wide areal dispersion of distal deposits, even if the reconstructed eruptive behavior characterized by an unsteady eruptive column alternating convective and collapsing phases is more typically sub-Plinian (or Vulcanian). In any case, they are orders of magnitude higher than the volumes of erupted material of the present-day paroxysms, which occasionally punctuate the eruptive activity of Stromboli (i.e., 10^3–10^5 m^3;[1,2]). The PET eruptive cycle therefore recurrently showed a higher explosivity compared with respect to the present-day activity of Stromboli, highlighting a different eruptive behavior of the volcano during its initial stages of evolution (Paleostromboli I).

Architecture of the magma plumbing system

The architecture of the magma plumbing system relevant to PET is derived from petrographic and mineralogical analysis combined with geobarometric calculations.

Our geobarometric calculations on pyroxenes[21] found pressure of crystallizations between 100 and 360 MPa (3.8–14 km), values which are similar to those of the present-day magmatic system of Stromboli. Also, a general deepening of the crystallization depth from the bottom to the top of PET (Table 3). Depths from the bottom of the PET sequence ($EU1_{A\text{-}B}$) indicates a very narrow range of crystallization (100–140 MPa, 3.8–5.3 km) which is almost entirely coincident with the present-day shallow reservoir where HP magma forms, as a result of cooling, crystallization and degassing of magma batches coming from the deeper portions of the plumbing system[2,7,8]. This shallow reservoir is made up of a largely hybridized zone due to mixing between HP magmas and the residing one[8], and is that feeds the present-day Strombolian persistent eruptive activity, only sporadically causing major explosions due to momentary obstructions or geometry changes of the conduit [e.g.,[25]]. The increase of the depth of crystallization is outlined by EU2 and EU3 clinopyroxenes, that respectively give values of 150–320 MPa (7.1–8.7 km) and 110–360 MPa (4–14 km). These depths are largely similar to those of the mid-crustal magma reservoir that feeds the LP magmas during the paroxysms of the present-day activity of Stromboli[7]. Unfortunately, thermobarometric investigations did not give reliable results for crystallization pressures of pyroxenes of units EU4 and EU5 to confirm eventually these occurrences. According to these data, if a constant Moho depth of ca. 15 km beneath the summit craters is assumed for the last 80 ka at Stromboli[23,26], the clinopyroxene barometry gives back a configuration of the plumbing system during the PET eruptive cycle

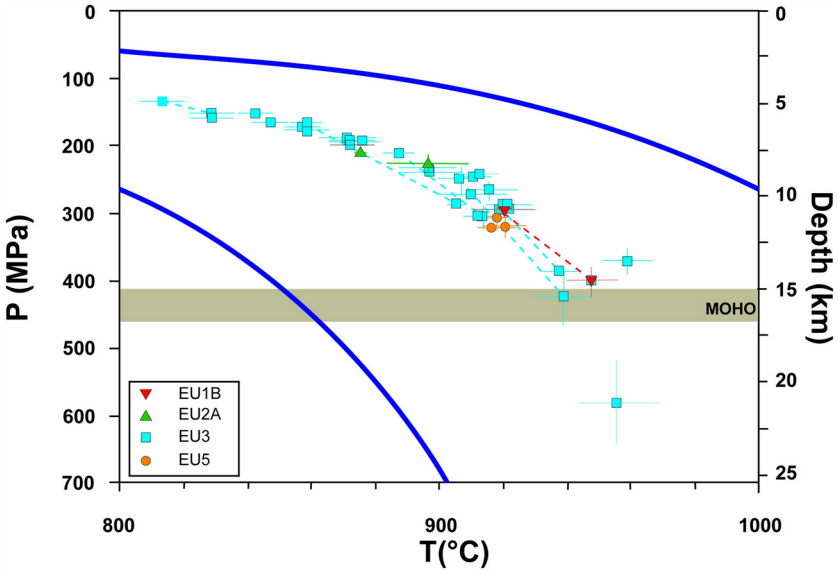

Fig. 7. Amp-TB2.xlsx P–T-d diagrams for the amphibole phenocrysts in the units of PET. Dashed lines connect homogeneous zonings within the same crystals. Colored error bars (without caps) show the 2σ values of the multiple-profile P–T conditions. Representative T (24 °C) and P (12%, relative) uncertainties of the method are reported as black-caped bars[20]. Mofo depth from[23,26]. Blu lines represent the limit of stability for the amphibole[20].

very similar to the present-day one, consisting of a polybaric plumbing system with a shallow (100–140 MPa, depths of 4–5 km) and a mid-crustal (up to 300 MPa, depths of 7–14 km) magma reservoirs.

Petrographically, PET has a distinctive presence of abundant (higher than 10 vol.%) amphibole crystals in equilibrium with the surrounding melt in most of the EUs, as indicated by the widespread lack of opaque (resorption) rims, which are commonly observed in mafic magmas. This is unique in the subaerial record of Stromboli, and differentiates the mineralogical assemblage and crystallization sequence of PET from that of the present-day of Stromboli, featuring olivine-oxides-pyroxenes-plagioclases. In the lowermost units EU1 and $EU2_{A\text{-}C}$, amphibole (up to 5 vol.%) occurs as microphenocrysts (< 300 µm) without a breakdown rim mostly in glomerophyric structures together with clinopyroxenes and plagioclases. This suggests that amphibole in PET is initially a secondary phase, crystallized at high P only in peripheral portions of the plumbing system. Conversely, amphibole reaches amounts up to 12 vol.% in unit EU3, the most energetic one of PET, as phenocrysts (> 500 µm of length) with absent breakdown rims. This suggests that amphibole was crystallized in equilibrium within the magma chamber, and after, during the EU3 eruption, and that magma ascent rate was high enough to prevent hydrogen loss from the crystallographic structure of the amphibole, which would have led to formation of breakdown (opaque) rims[19]. Amphibole phenocrysts with evident breakdown rims are present again in EU5 (up to 5 vol.%), suggesting that these crystals were not in equilibrium with the surrounding magma during the eruption. Unfortunately, technical issues did not allow us to gain reliable thermobarometric reliable pressure constraints for the scarce amphiboles of unit EU5. We advance the hypothesis that they are residual within the magma plumbing system of PET after the large magnitude eruption recorded by EU3. For units EU1-EU4, the amphibole thermobarometer of[20] provides pressures of equilibration of 130–420 MPa corresponding to depths of 5–16 km below the summit craters (apart of an anomalous value of ca. 22 km for one of the samples) is excluded (Fig. 7). This range provides a picture of a widely vertically developed plumbing system during the PET eruptive cycle, extending from the depths of the Moho (15–17 km) to the upper boundary of the deeper magma reservoir feeding the present-day activity of Stromboli.

Experimental results in basaltic magmas show that amphibole crystallization is favored by free-H_2O contents ≥ 6 wt% and values of Na_2O/K_2O ratio for hosting magmas ≥ 0.9[27–29]. Although the second condition is respected within the whole PaleoStromboli I eruptive epoch and in the PET sequence (Table S1), the higher most contents of dissolved water for present-day activity are only between 2.7 and 3.5 wt%[7]. The needed higher H_2O content needed for the crystallization of amphiboles in PET magmas could be then related to: (1) greater availability of water in the melting source, or (2) different physical conditions in the plumbing system. Recently,[30] proposed that most of the water available in the magma system of Stromboli would derive from the breakdown and melting of amphibole in the mantle source, with a minor component deriving from the subduction and dehydration of sediments in the subduction zone. Following this hypothesis, the greater availability of water during PET eruptions could be attributed to a higher degree of partial melting, maybe too high to be considered realistic. Nonetheless, the PET volcano stratigraphy outlined the occurrence of alternating explosive eruptions and quiescent periods recorded in erosional unconformities and paleosols. We put forward the idea that the higher amount of H_2O in the magma plumbing system of PET could be attributed to closed- or partially-closed conduit conditions, able to hinder the exsolution of water in the lower portions of the plumbing system (10–

12 km) and to increase the water pressure in the magma and thus favoring the crystallization conditions for amphibole.

Magma storage and (pre-eruptive) ascent dynamics

In order to assess the pre-eruptive dynamics which led to the highly explosive PET cycle, it is crucial to note that processes able of altering the pristine magma composition at the source or crustal assimilation are absent. Although an increase in potassium and incompatible elements is observed for the Paleostromboli I activity, as suggested by[2], no significant variations are found in PET (Fig. 3). In addition, the highly evolved compositions reached by these magmas, part of the high-K calc-alkaline series, do not exhibit a systematic increase in Sr isotope ratios, both in whole rock and in mineral compositions[2]. This suggests that this high evolutionary degree is linked to simple fractional crystallization of a mafic mineral assemblage (olivine, clinopyroxene, plagioclase, Fe–Ti-oxides, apatite ± biotite) in the more evolved melts, with a solid fractionation of 55–76%[2,31].

In recent decades, plagioclase has emerged as a reliable crystallographic phase for deciphering pre- and syn-eruptive dynamics during magma storage and ascent, encompassing processes like quiet cooling, crystal fractionation, magma mixing, volatile ingress and magma recharge, and then giving information about physical and chemical conditions of the crystallizing melts, but also for the detection of volcano-tectonic processes affecting the magmatic system[32–37]. Moreover, variations in the frequency/abundance of different plagioclase textures across a volcanic-stratigraphic succession can help in the definition of evolving scenarios.

Plagioclase crystals of PET show oscillatory zoning with small variations of the An content ($<\Delta An_8$) and two different amplitude of oscillations ($\Delta An_{1\text{-}4}$ and $\Delta An_{5\text{-}8}$) at fairly constant FeO (Fig. 5). This texture is typical of magmatic reservoirs characterized by minor physical and chemical gradients and suggests limited crystal movements in a quiet environment[38]. The $\Delta An_{1\text{-}4}$ pattern may be associated to kinetics of crystallization at the crystal/melt interface within a chemically and physically unperturbed system[38]. On the other hand, $\Delta An_{5\text{-}8}$ at constant FeO is indicative of small changes of the physical and chemical conditions of the magmatic system not sufficient to induce major dissolution episodes, as crystals able to move within a plumbing system not significantly vertically-developed[36,38].

Oscillatory zoning is often superimposed by layers of melt inclusions aligned along the crystallographic directions, where the nearby Pl zones show a significant An content increase (up to ΔAn_{18}) at constant FeO (Fig. 5). The mechanism behind the entrapment of melt inclusions in plagioclase is still not fully understood, but two different dynamics are currently invoked in generating a rapid increase of An content in the crystallizing plagioclase: (1) sudden depressurization of the magma reservoir where plagioclases are crystallizing in water-saturated conditions[37,39,40]; (2) increase of the water content, i.e. by gas-flushing from depth[41,42]. In PET products, plagioclases do not show evidence of gas-flushing, which would be outlined by an increase of FeO content in correspondence of the melt inclusions alignment[37,38]. So, we put forward the idea that melt inclusions in the PET plagioclases are related to a rapid depressurization undergone by the magma reservoir where plagioclases were crystallizing. This case, already observed in other volcanic systems[32,34,35,37], would be associated with an increased growth rate of plagioclases, leading to incorporation of small drops of melt perpendicularly to the crystal growth planes. It is notable that up to four parallel alignments of melt inclusions are found in some crystals, especially in EU3, which suggests that the magma plumbing system experienced a corresponding number of decompression episodes.

Plagioclases can also register major physical perturbations of the magma system during the complex phases preceding an eruption by means of disequilibrium textures, sometimes coupled with compositional changes[43,44]. Experimental petrology has demonstrated that different ascent rates at isothermal conditions are able to reduce the stability field of plagioclase, provoking the development of resorbed cores[40,42]. Plagioclase crystals of PET also present envelopes of resorption at the rims (Fig. 5), where concordant increases of the An and FeO contents (up to ΔAn_8 and up to 2 wt.%, respectively) are recorded. These envelopes of resorption are generally related to the injection of a fresh magma, i.e. a magma with composition similar to the host one but slightly more basic, hot and volatile-rich[32,34,35,37]. This magma recharge is able to suddenly modify the chemical and physical conditions of the host magma and to efficiently produce a chemical mixing with the residing magma[38–40,42,43]. Therefore, the contemporaneous increases of An and FeO contents in correspondence of the envelopes of resorption are due to the occurrence of magma injection and mixing. Envelopes of resorption in PET plagioclases are usually encircled by a very thin (< 50 μm) "shell" of oscillatory zoning, suggesting that the ingress of the new magma into the plumbing system can be considered the trigger of the eruption itself.

Triggering mechanisms

The widespread occurrence of medium to highly vesicular juvenile fragments and irregular, plastically deformed bombs throughout PET (and the paucity of ash) indicates that the main mechanism driving magma fragmentation at the onset and during the whole eruptive activity was purely magmatic, with no substantial interaction between magma and external water. As such, the driving pressure needed for eruption initiation in a magmatic system is given by the magma overpressure (P_0) minus the pressure required for maintaining open the dyke (ΔP_{0m}), which are balanced by the tensile strength of the rocks (T_0, in the case of closed conduit), the weight of magma column (i.e. magmastatic loading, ρgh), the lithostatic stress (σ_l) and the resisting forces per unit area (R_p;[44]):

$$P_0 - \Delta P_{0m} = T_0 + \rho gh + \sigma_l + R_p$$

Irrespective if we are in closed or open conduit conditions, the main variables that can abruptly alter the equilibrium and trigger a transition to eruption are P_0 (magma overpressure) and σ_l (component of the lithostatic stress). Initiation of the eruption can be then triggered by an increase in magma overpressure (magmatic triggering), a decrease of lithostatic pressure (non-magmatic trigger), or a combination of them. In

the case of PET, the petrologic and compositional data suggest that the triggering of eruptive event is mainly due to the decompression of the feeding system, except for EU1 in which both a magma recharge [as suggested by plagioclase textures and by the mingled hand-sized juvenile clasts] and a reduction of the lithostatic load [(as shown by the prevalence of melt inclusions alignments within plagioclase (Fig. 6)], concurred in eruption triggering.

The onset of the PET eruptive cycle witnessed the eruption of basalt and basaltic andesite products ($EU1_A$), signaling an evident compositional shift from andesites of the previous Paleostromboli I units (Malpasso fm.; Fig. 3C). This is a major signal that the magma plumbing system was rejuvenated by the arrival of a new and more mafic magma, which mingled and (eventually) mixed with the residing, as also testified by the occurrence in unit $EU1_B$ of banded juveniles with dark basaltic andesite and light dacite portions (Fig. 2C). The predominance of mingling (mechanical) over mixing (chemical) processes in EU1 is highlighted by the presence of only 9–14% of plagioclase phenocrysts presenting envelopes of resorption (texture typical of magma mixing). Nonetheless, the presence of associated melt inclusions (41–48%; Fig. 6) and resorbed cores (22–29%; Fig. 6) in the plagioclases of EU1 also suggests an important event of decompression of the feeding system before eruption. One possible explanation for this is the unloading of the feeding system induced by a lateral collapse of the volcano, which is a process that occurred repeatedly in the eruptive history of Stromboli, as in the area of Le Schicciole–Rina Grande where PET crops out. However, this remains only a hypothesis since there is little geological evidence of a structural collapse of about 80 ka (with the exception of a possible debris avalanche deposit at the base of PET), the traces of which would be covered by younger deposits (or obliterated by more recent collapses) or would be found along the submarine flanks of the volcano. The depressurization of the feeding system as an eruptive trigger is also dominant in EU2, as shown by the total amount of plagioclase characterized by melt inclusions (25–46%; Fig. 6) and resorbed cores (19–36%; Fig. 6). In addition, the increasing of Oscillatory-Zoned plagioclases up to 31–34% (Fig. 6) suggest the unique involvement in the eruptive events of the magma stored in the shallow reservoir (0.5–4 km; Table 3), as also confirmed by double oscillatory zoning in plagioclases (up to 31%; Fig. 6). Here, the magma intruded during EU1 has efficiently mingled and then chemically homogenized through time, as also testified by the similar whole rock and glass compositions of EU1 and EU2 (Fig. 3).

During the PET eruptive cycle, it is evident that depressurization of the magma plumbing system becomes the main triggering mechanism. Lowering of the lithostatic stress was long claimed to play a fundamental role in triggering volcanic eruptions and in controlling their dynamics [e.g.,[37,44,48]]. Changes of stress acting on both edifices and magma chambers can be usually related to processes with different characteristic timescales. In particular, the occurrence of tectonic earthquakes and lateral collapses are short-term processes that can affect eruptive style transition[48]. Concerning earthquakes, present day seismic activity is not able to significantly influence the activity of the volcano[2], so we assume the same behavior also at time of PET. The reduction of the lithostatic load in the previous equation can be given also by the edifice lateral spreading, defined as the lateral deformation of a volcanic edifice along a basal ductile layer that deforms under the volcano weight (e.g.[49,50]). In the Stromboli case, there are no data on possible spreading of the volcano edifice, which is largely submerged. In any case, a lateral gravitational spreading of a 3000 m-high volcano (considering its submerged portion) is more than probable and needs to be accurately considered when dealing with the rupture of the feeding system equilibrium. This is because a sudden spreading jerk has the same effect that producing an overpressure in the system, by reducing the σ_l in the previous equation. During the recent activity at Stromboli, it has been also proposed that, at least for major explosions, decompression of the magma plumbing system could be also attributed to modification in the geometry of the conduit and can then trigger a very fast magma ascent from the deeper most level of the feeding system[25]. The combination of all the petrological, geochemical and mineralogical evidences presented here suggest that at PET the lowering of the lithostatic stress could be attributed to volcano-tectonic events of different scale. In particular, the unusual evolved compositions of whole rock and glasses of PET and the unique presence of amphibole crystals lead us to put forward the idea that the eruption triggering can be related to phases of opening of the conduit system after a period of closure. Closed-conduit conditions are not usual at Stromboli, which has been generally considered as an open-conduit system able to give almost continuous activity.

The EU3, which records the most explosive eruption of PET, is characterized by dacitic glasses, which are among the most evolved in the entire geological record of Stromboli (Fig. 3A). This is consistent with wide fractionation occurred in closed-conduit conditions during a prolonged quiescence period testified by the paleosol at the base of the unit. Plagioclase textures (melt inclusions and resorbed cores up to 68%) suggest that this eruption was triggered by a sudden decompression, which was able to recall magma from the deeper portions of the plumbing system. The ingress of a new more mafic, hotter and gas-rich magma is therefore subsequent to a main triggering event and is a consequence of the emptying/eruption of the magma occupying the shallow feeding system. Such a dramatic modification of the physical parameters within the feeding system in registered by the opaque rims found only in the amphiboles of EU3. The final arrival of this new magma is also registered by the highest frequency of envelopes of resorption (up to 24%) in the whole PET (Fig. 6). This magma mingled and then efficiently mixed with the residing one, causing a shifting of whole rock compositions from andesites to basaltic andesites (Fig. 3C), and the emission of banded and grey pumices (Fig. 2C).

The EU5 registers a substantial change of pre-eruptive conditions, with magmas which again shifted their compositions toward more mafic terms. The absence of dusty sieve textures at plagioclase rims and the occurrence of MI layers in different places within the crystals, indicate that no magma mixing occurred and that the trigger mechanism likely was a decompression of the system. Taking into account the low crystallinity of erupted products (< 25 vol. %), we put forward the idea that EU5 records the emptying of intermediate-shallow portions (down to 12 km of depth) of the plumbing system due to very rapid magma ascent induced by a sudden decompression. As mentioned before, a very plausible hypothesis is that this decompression is induced by a lateral collapse of the edifice. This would be consistent with the sharp angular unconformity and thick lahar

deposits recognized at the base of unit EU5, which record the massive erosion and reworking processes occurred during the phase of large-scale re-organization of the volcanic system subsequent to the major structural collapse. However, also in this case, there is no direct evidence in the field of a structural collapse in this stratigraphic window, even if it must be noticed that such traces could easily have been removed by the subsequent major collapse (sc2 in Fig. 1A) occurred in the area of Le Schicciole–Rina Grande in the time interval between 34 and 26 ka[2].

In summary, we put in evidence of occurrence of recurrent phases of magma differentiation + decompression of the plumbing system + magma rejuvenation during the PET cycle at the transitions between units EU1-EU2, EU2-EU3, and EU4-EU5. The volcanic system was predominantly closed, so that to favor the crystallization of amphibole within the magma plumbing system during the corresponding quiescence periods. The occurrence of quiescence periods and opening phases highlighted by the presence of paleosols and interlayered breccia units within PET suggests that probably the configuration of the shallow plumbing system was not the same as for the present-day activity. The periods of quiescence can explain the extensive crystal fractionation processes at shallow and intermediate levels of the plumbing system during the PET eruptive cycle. Re-openings of the conduit and decompression of the plumbing system induced the arrival of new magmas from the deep portions of the plumbing system. The more is the depressurization, the deeper is the interested portion of the plumbing system. This model is in accordance with[8], who proposed that decompression of the deeper reservoir of the magmatic system is the usual trigger for paroxysms at Stromboli, even if the scale of the eruptions of PET is much greater.

Conclusive remarks

The interdisciplinary study of the deposits related to the Petrazza (PET) eruptive cycle (75–77 ky), during the PaleoStromboli eruptive epoch, has provided valuable insights into the configuration and processes within the magma plumbing system during the largest magnitude explosive eruptions of Stromboli (and among the most explosive in the entire Aeolian archipelago). Specifically:

1. The long-lasting explosive eruptive cycle of PET is characterized by five Eruption Units (EU1-EU5), further subdivided into distinct eruptive pulses, and separated by quiescent periods. EU3 and potentially EU5 are associated with sub-Plinian to Plinian eruptions, with deposits dispersed extensively across the Tyrrhenian Sea and Italian mainland.
2. Geobarometric and mineralogical investigations suggest a polybaric system extending beyond 14 km in depth, resembling the present-day configuration at Stromboli. However, the presence of amphibole phenocrysts in equilibrium at depths of 5–16 km indicates slightly different crystallization conditions, potentially facilitating increased water content in the melt (e.g., within a closed-conduit system).
3. Textural and compositional analyses of plagioclase suggest that the primary eruptive triggers in PET can be attributed to decompression of the feeding system, deep magma recharge, or a combination of both. The depressurization of the plumbing system is here linked to a transition from closed to open-conduit conditions, possibly in association with lateral collapse events. The largest magnitude explosive eruptions of PET are associated with a significant decompression, capable of mobilizing amphibole-bearing mafic magma from deeper portions of the plumbing system.

Methods

Sampling and methods

Geological survey and sampling

Lithostratigraphic and sedimentological analysis, volcanological interpretation and sampling for petrochemical investigation of the Petrazza pyroclastic succession was carried out by means of classical methods of outcrop description and stratigraphic logging based on lithostratigraphy and lithofacies analysis ([16,52] for reviews). Distinct eruption units (EUs) have been defined as the products of single eruptions or eruptive phases (sensu[52]), each one characterized by a distinctive lithofacies association and/or by boundaries representing a significant volcanic quiescence (erosion surfaces, angular unconformities, paleosols and/or reworked/detrital deposits;[15]). An eruptive cycle is a sequence of distinct eruption units separated by unconformities (cf.[52]). Within an EU, we recognize a number of depositional units corresponding to the pyroclastic material deposited during pulses of pyroclastic density currents or fall, lahar or even erosional reworking and lahars. Distinct depositional units are delimited by evidence of interruptions of deposition at a shorter time scale than those corresponding to the eruption units, that is minor erosive surfaces or angular unconformities, paleosols, reworked beds) or other sedimentological features (e.g. fine ash or lithic-rich beds, sharp grain-size variations).

A total of 30 rock samples were collected for petrochemical investigation of the Petrazza succession, and also of the other lithostratigraphic units of the Paleostromboli I volcano (Malpasso, Vallone del Monaco, La Petrazza 2 fms.; cf.[2]) to have a wider picture on the eruptive dynamics of this time-stratigraphic window. Samples for the Malpasso fm. by[53] are also considered to complete the dataset. In addition, pumice lapilli of the Petrazza succession found on Panarea Island have been sampled to assess the proximal-to-distal correlations of this unit. Whole rock data for all the collected samples are reported in Table S1.

Analytical conditions for whole rock and microanalytical investigations

Whole rock compositions in terms of major and some trace elements were obtained at the Dipartimento di Biologia, Ecologia e Scienze della Terra of the University of Calabria (Italy) by means of a Bruker S8 Tiger XRF spectrometer on powder pellets with matrix effect corrections. The precision, measured as percentage difference between certified and measured composition of standards analyzed as unknown samples, was always < 5% for major elements and 10% for trace elements. FeO was determined by titration. Loss on ignition was determined

by gravimetric methods and corrected for Fe^{2+} oxidation. The sum of oxides was always higher than 95%. All the analyses were re-calculated for a sum of 100%.

On 27 selected rock samples, polished thin sections were obtained. Mineralogical and petrographic observations were performed by means of optical and polarized microscopy. Compositional core-to-rim profiles were executed on 40 plagioclase crystals on polished, graphite-coated thin sections by means of Electron MicroProbe Analyzer (EMPA). Plagioclase crystals were selected on the basis of the representativeness of their texture within each sample. Only phenocrysts a length > 500 μm along the *c* axis were considered for this type of analysis; in this regard, only plagioclase clearly in equilibrium with the surrounding liquid have been considered, avoiding the (small) number of plagioclase antecrysts and xenocrysts. All compositional data on plagioclase are reported in Supplementary Table S4. We used the JEOL JXA-8230 of SILA-CM2 lab at the University of Calabria, equipped with 5 WDS and one EDS spectrometers. WDS analyses were carried out with an accelerating voltage of 15 kV and probe current of 10 nA. Count times were 15 s for Na and 30 s for other elements.

The abundance of each texture on each sample has been related to its stratigraphic (and then temporal) position of the volcanic sequence of Petrazza, considering only phenocrysts > 500-μm-long (on the *c* axis) and avoiding the counting antecrysts or xenocrysts (i.e., crystals clearly not in equilibrium with the surrounding magma) and portions of crystal. The results of this count on more than 3500 crystals are represented in Fig. 6.

Amphibole thermobarometry: methods and results

Single amphibole (Amp) thermobarometry were applied to phenocrysts found in rock samples of the Petrazza units $EU1_B$, $EU2_A$, EU3 and EU5 following the protocol of[20].

BSE imaging and core-rim profile EMPA analyses were performed for a total of 28 Amp phenocrysts. EMPA analyses has been performed in spot mode (beam size ~ 1 μm) with steps of 5-40 μm as a compromise between the size and homogeneity of the crystals. The quality of each Amp composition was checked using AMFORM.xlsx[54]. The identification of the homogenous amphiboles and intra-crystal domains, and related thermobarometric calculations, were performed using the spreadsheet Amp-TB2.1.xlsx[20]. The average pressure (P), temperature (T) oxygen fugacity (fO_2) and water content in the melt (H_2Omelt) and their uncertainties (expressed as standard deviation of multiple calculations, σ) was calculated for a total of 34 homogenous amphiboles and intra-crystal domains (Table 3 and Fig. 7).

Data availability

Data is provided within the manuscript or supplementary information files.

Received: 5 February 2024; Accepted: 12 November 2024
Published online: 22 November 2024

References

1. Rosi, M. et al. Stromboli volcano, Aeolian Islands (Italy): Present eruptive activity and hazards. *Geol. Soc., London, Mem.* **37**, 473–490 (2013).
2. Francalanci, L. et al. Eruptive, volcano-tectonic and magmatic history of the Stromboli volcano (north-eastern Aeolian archipelago). *Geol. Soc. Lond. Mem.* **37**, 397–471 (2013).
3. Hornig-Kjarsgaard, I. et al. Geology, stratigraphy and volcanological evolution of the island of Stromboli, Aeolian arc, Italy. *Acta Vulcanol.* **3**, 21–68 (1993).
4. Lucchi, F. et al. Geological evidence for recurrent collapse-driven phreatomagmatic pyroclastic density currents in the Holocene activity of Stromboli volcano, Italy. *J. Volcanol. Geotherm. Res.* **385**, 81–102 (2019).
5. Tibaldi, A. Multiple sector collapses at Stromboli volcano, Italy: how they work. *Bull. Volcanol.* **63**, 112–125 (2001).
6. Francalanci, L., Tommasini, L., Conticelli, S. & Davies, G. R. Sr. isotope evidence for new magma input and short residence time in the XX century activity of Stromboli volcano. *Earth Planet. Sci. Lett.* **167**, 61–69 (1999).
7. Métrich, N., Bertagnini, A. & Di Muro, A. Conditions of magma storage, degassing and ascent at Stromboli: new insights into the volcano plumbing system with inferences on the eruptive dynamics. *J. Petrol.* **51**, 603–626 (2010).
8. Landi, P. et al. Inferences on the magmatic plumbing system at Stromboli volcano (Italy) from trace element geochemistry of matrix glasses and minerals in different types of explosive eruptions. *Contrib. Mineral. Petrol.* **177**, 96. https://doi.org/10.1007/s00410-022-01962-1 (2022).
9. Lucchi, F., Keller J. & Tranne, C. A. Regional stratigraphic correlations across the Aeolian archipelago. *Geol. Soc., London, Mem.* **37**, 55–81 (2013).
10. Morche, W. Tephrochronologie der AolischenInseln. Unpublished PhD thesis, Albert-Ludwigs-Universität Freiburg, Germany (1988).
11. Lucchi, F., Tranne, C. A., Calanchi, N., Keller, J. & Rossi, P. L. The stratigraphic role of marine deposits in the geological evolution of the Panarea volcano (Aeolian Islands, Italy). *J. Geol. Soc. Lond.* **164**(5), 983–996 (2007).
12. Wulf, S., Kraml, M., Brauer, A., Keller, J. & Negendank, J. F. W. Tephrochronology of the 100 ka lacustrine sediment record of Lago Grande di Monticchio (southern Italy). *Quat. Int.* **122**, 7–30 (2004).
13. Kraml, M. Laser 40Ar/39Ar-datierungen an distalenmarinentephren des jungquartären mediterranean vulkanismus (Ionisches Meer, Meteor-Fahrt 25/4). *PhD thesis*, Albert Ludwigs-Universität Freiburg, Germany (1997).
14. Paterne, M., Guichard, F., Labeyrie, J. Explosive activity of the South Italian volcanoes during the past 80,000 years as determined by marine tephrochronology. *J. Volcanol. Geotherm. Res.* **34**, 153–172. https://doi.org/10.1016/0377-0273(88)90030-3 (1988).
15. Rosi, M. The island of Stromboli. *Rend. Soc. Ital. Mineral. Petrol.* **36**, 345–368 (1980).
16. Lucchi, F. Stratigraphic methodology for the geological mapping of volcanic areas: insights from the Aeolian archipelago (Southern Italy). In *The Aeolian Islands Volcanoes* Vol. 37 (eds. Lucchi, F. et al.) 37–53 (Geological Society, 2013).
17. Salvioli-Mariani, E., Mattioli, M., Renzulli, A. & Serri, G. Silicate melt inclusions in the cumulate minerals of gabbroic nodules from Stromboli volcano (Aeolian Islands, Italy): main components of the fluid phase and crystallization temperatures. *Mineral. Mag.* **66**, 969–984 (2002).
18. Mattioli, M. et al. Sub-volcanic infiltration and syneruptive quenching of liquids in cumulate wall-rocks: the example of the gabbroic nodules of Stromboli (Aeolian Islands, Italy). *Mineral. Petrol.* **78**, 201–230 (2003).
19. Rutherford, M. J. & Devine, J. D. Magmatic conditions and magma ascent as indicated by hornblende phase equilibria and reactions in the 1995–2002 Soufrière Hills Magma. *J. Petrol.* **44**, 1433–1453 (2003).

20. Ridolfi, F., Almeev, R. R., Ozerov, A. Y. & Holtz, F. Amp-TB2 protocol and its application to amphiboles from recent, historical and pre-historical eruptions of the Bezymianny Volcano, Kamcahtka. *Minerals* **13**(11), 1394 (2023).
21. Wang, X. et al. A new clinopyroxene thermobarometer for mafic to intermediate magmatic systems. *Eur. J. Mineral.* **33**(5), 621–637 (2021).
22. Ridolfi, F., Puerini, M., Renzulli, A., Menna, M. & Toulkeridis, T. The magmatic feeding system of El Reventador volcano (Sub-Andean zone, Ecuador) constrained by texture, mineralogy and thermobarometry of the 2002 erupted products. *J. Volcanol. Geotherm. Res.* **176**(1), 94–106 (2008).
23. Martinez-Arevalo, C., Musumeci, C. & Patanè, D. Evidence of a partial melt zone beneath Stromboli volcano (Italy) from inversion of teleseismic receiver functions. *Terra Nova* **21**, 386–392. https://doi.org/10.1111/j.1365-3121.2009.00894.x (2009).
24. Sulpizio, R., Costa, A., Massaro, S., Selva, J. & Billotta, E. Assessing volumes of tephra fallout deposits: A simplified method for data scarcity case. *Bull. Volcanol.* **86**, 62. https://doi.org/10.1007/s00445-024-01753-5 (2023).
25. Viccaro, M. et al. Shallow conduit dynamics fuel the unexpected paroxysms of Stromboli volcano during the summer 2019. *Sci. Rep.* **11**(1), 266 (2021).
26. Cigolini, C., Laiolo, M. & Coppola, D. Revisiting the last major eruptions at Stromboli volcano: inferences on the role of volatiles during magma storage and decompression. *Geol. Soc. Lond. Spec. Publ.* **410**(1), 143–177 (2015).
27. Krawczynski, M. J., Grove, T. L. & Behrens, H. Amphibole stability in primitive arc magmas: effects of temperature, H_2O content, and oxygen fugacity. *Contrib. Mineral. Petrol.* **164**(2), 317–339 (2012).
28. Melekhova, E., Blundy, J., Robertson, R. & Humphreys, M. C. Experimental evidence for polybaric differentiation of primitive arc basalt beneath St. Vincent, Lesser Antilles. *J. Petrol.* **56**(1), 161–192 (2015).
29. Bonechi, B., Perinelli, C., Gaeta, M., Tecchiato, V. & Granati, S. F. Experimental constraints on amphibole stability in primitive alkaline and calc-alkaline magmas. *Period. Mineral.* **86**, 231–245 (2017).
30. Bouvier, A. S., Rose-Koga, E. F. & Chapuis, A. Deciphering degassing and source effects in Cl isotopes in melt inclusions: the possible role of amphibole in the magma source of Stromboli (Aeolian Island Arc). *Front. Earth Sci.* **9**, 793259 (2022).
31. Francalanci, L., Manetti, P. & Peccerillo, A. Volcanological and magmatological evolution of Stromboli volcano (Aeolian islands): the roles of fractional crystallisation, magma mixing, crustal contamination and source heterogeneity. *Bull. Volcanol.* **51**, 355–378 (1989).
32. Viccaro, M. et al. Crystal residence time from trace element zoning in plagioclase reveal changes in magma transfer dynamics at Mt. Etna during the last 400 years. *Lithos* **248–251**, 309–323. https://doi.org/10.1016/j.lithos.2016.02.004 (2016).
33. Muro, Di. et al. The shallow plumbing system of Piton de la Fournaise volcano (La Réunion Island, Indian Ocean) revealed by the major 2007 caldera forming eruption. *J. Petrol.* **55**, 1287–1315. https://doi.org/10.1093/petrology/egu025 (2014).
34. Nicotra, E., Viccaro, M., De Rosa, R., and Sapienza, M. (2014). Volcanological evolution of the Rivi-Capo Volcanic complex at Salina, Aeolian Islands: magma storage processes and ascent dynamics. *Bull. Volcanol.* **76**, 840–864 (2014).
35. Nicotra, et al. Timescales of pre-eruptive magmatic processes at Vulcano (Aeolian Islands, Italy) during the last 1000 years. *Lithos* **316–317**, 347–365. https://doi.org/10.1016/j.lithos.2018.07.028 (2018).
36. Nicotra, E. & Viccaro, M. Unusual magma storage conditions at Mt. Etna (Southern Italy) as evidenced by plagioclase megacryst-bearing lavas: implications for the plumbing system geometry and summit caldera collapse. *Bull. Volcanol.* **74**, 795–815. https://doi.org/10.1007/s00445-011-0566-9 (2012).
37. Nicotra, E., Minniti, M., Donato, P. & De Rosa, R. Insights into the eruptive dynamics of small caldera-forming eruptions: the case study of the Welded Scoriae of Vulcano (Aeolian Islands, Italy). *Front. Earth Sci.* **8**, 223. https://doi.org/10.3389/feart.2020.00223 (2020).
38. Streck, M. J. Mineral textures and zoning as evidence for open system processes. In *Minerals, Inclusions and Volcanic Processes. Reviews Miner. Geochem.*, Vol. 69 (eds. Putirka, K. D. & Tepley, F. J. III) 595–622 (Mineralogical Society of America, 2008).
39. Nielsen, R. L. et al. Melt inclusions in high-An plagioclase from the Gorda Ridge: an example of the local diversity of MORB parent magmas. *Contrib. Mineral. Petrol.* **122**, 34–50 (1995).
40. Nelson, S. T. & Montana, A. Sieve-textured plagioclase in volcanic rocks produced by rapid decompression. *Am. Mineral.* **77**, 1242–1249 (1992).
41. Nicotra, E., Viccaro, M., Ferlito, C., and Cristofolini, R. Influx of volatiles into shallow reservoirs at Mt. Etna volcano (Italy) responsible for halogen-rich magmas. *Eur. J. Mineral.* **22**, 121–138. https://doi.org/10.1127/0935-1221/2010/0022-1991 (2010).
42. Tsuchiyama, A. Dissolution kinetics of plagioclase in the melt of the system diopside-albite-anorthite, and the origin of dusty plagioclase in andesites. *Contrib. Mineral. Petr.* **89**, 1–16. https://doi.org/10.1007/bf01177585 (1985).
43. Nakamura, M. & Shimakita, S. Dissolution origin and syn-entrapment compositional changes of melt inclusions in plagioclase. *E. Planet. Sci. Lett.* **161**, 119–133. https://doi.org/10.1016/s0012-821x(98)00144-7 (1998).
44. Massaro, S. et al. Understanding eruptive style variations at calc-alkaline volcanoes: the 1913 eruption of Fuego de Colima volcano (Mexico). *Bull. Volcanol.* **80**, 62 (2018).
45. Rivalta, E. et al. A review of mechanical models of dike propagation: Schools of thought, results and future directions. *Tectonophysics* **638**(7), 1–42 (2015).
46. Melnik, O. & Sparks, R. S. J. Controls on conduit magma flow dynamics during lava dome building eruptions. *J. Geophys. Res.* **110**, B02209. https://doi.org/10.1029/2004JB003183 (2005).
47. Amoruso, A. & Crescentini, L. Shape and volume change of pressurized ellipsoidal cavities from deformation and seismic data. *J. Geophys. Res.* **114**, B02210 (2009).
48. Sulpizio, R., and Massaro, S. Influence of stress field changes on eruption initiation and dynamics: a review. *Front. Earth Sci.* **5**, 18 (2017).
49. Norini, G. & Acocella, V. Analogue modeling flank instability at Mt. Etna: undestranding the driving factors. *J. Geophys. Res. Solid Earth* **116**, B7 (2011).
50. Acocella, V. et al. Why does a mature volcano need new vents? The case of the new Southeast Crater at Etna. *Front. Earth Sci.* **4**, 56 (2016).
51. Peccerillo, A. & Taylor, S. R. Geochemistry of Eocene calc-alkaline volcanic rocks from the Kastamonu Area, Northern Turkey. *Contrib. Mineral. Petr.* **58**, 63–81. https://doi.org/10.1007/bf00384745 (1976).
52. Lucchi, F. On the use of unconformities in volcanic stratigraphy and mapping: Insights from the Aeolian Islands (southern Italy). *J. Volcanol. Geotherm. Res.* **385**, 3–26 (2019).
53. Niceforo, G. Petrografia e geochimica dei magmi del Paleostromboli. *Unpublished thesis*. Università della Calabria, Italy (2000).
54. Ridolfi, F., et al. AMFORM, a new mass-based model for the calculation of the unit formula of amphiboles from electron microprobe analyses. *Am. Mineralog.* **2018**, 103–7 (2018)

Acknowledgements

This work is part of the PhD Thesis of MM. Authors are thankful to Laurent Geoffroy for its editorial handling, and to Lucia Gurioli and an anonymous reviewer for their useful comments, which made the manuscript more readable. This paper has been financed by the RETURN PRoject "Multi-Risk sciEnce for resilienT commUnities undeR a changiNg climate (RETURN)", Project code PE00000005, CUP H93C22000610002, financed by PNRR, Mission 4 "Instruction and REsearch" - Component 2 "From research to the business" - Investment 1.3, financed

by European Union - NextGenerationEU - EXPERIFLOWS Project, of which E.N. is the Principal Investigator.

Author contributions

F.L., coordinated and performed together with R.S., C.A.T and E.N. the new geological survey and relative rock sampling of Petrazza at Stromboli island. E.N. and F.L. conceived the paper. E.N. interpreted the petrological data, and prepared the main manuscript together with F.L. M.M. was responsible for the entire acquisition and analysis of data (e.g., XRF, EPMA) and prepared all the supplementary files, the tables and Figs. 4–5. F.R. elaborated the geobarometric data on amphiboles and prepared Fig. 7. R.S. and C.A.T. improved the manuscript quality giving hints on the eruptive mechanisms. All the authors revised the final version of the manuscript.

Competing interests

The authors declare no competing interests.

Additional information

Supplementary Information The online version contains supplementary material available at https://doi.org/10.1038/s41598-024-79851-9.

Correspondence and requests for materials should be addressed to E.N. or F.L.

Reprints and permissions information is available at www.nature.com/reprints.

Publisher's note Springer Nature remains neutral with regard to jurisdictional claims in published maps and institutional affiliations.